Journal of Biomedical Optics

BiomedicalOptics.SPIEDigitalLibrary.org

Natural zeolite for adsorbing and release of functional materials

Vladimir Ararat Hovhannisyan
Chen-Yuan Dong
Feng-Jie Lai
Nan-Shan Chang
Shean-Jen Chen

SPIE.

Vladimir Ararat Hovhannisyan, Chen-Yuan Dong, Feng-Jie Lai, Nan-Shan Chang, Shean-Jen Chen, "Natural zeolite for adsorbing and release of functional materials," *J. Biomed. Opt.* **23**(9), 091411 (2018), doi: 10.1117/1.JBO.23.9.091411.

Natural zeolite for adsorbing and release of functional materials

Vladimir Ararat Hovhannisyan,[a] Chen-Yuan Dong,[b] Feng-Jie Lai,[c] Nan-Shan Chang,[a] and Shean-Jen Chen[d,*]
[a]National Cheng Kung University, Institute of Molecular Medicine, Tainan, Taiwan
[b]National Taiwan University, Department of Physics, Taipei, Taiwan
[c]Chi Mei Medical Center, Department of Dermatology, Tainan, Taiwan
[d]National Chiao Tung University, College of Photonics, Tainan, Taiwan

Abstract. Using multiphoton microscopy (MPM), we demonstrated that effective inducing of two-photon excited luminescence and second-harmonic generation signals in nano/microparticles of clinoptilolite type of zeolite (CZ) by femtosecond near-infrared laser excitation can be successfully utilized in multiphoton imaging of the drug adsorption processes. Adsorption of photodynamic active dyes (hypericin, chlorin e_6, methylene blue, and fluorescein) and their release from CZ pores in the presence of biomolecules, such as collagen from bovine Achilles tendon, albumin, and hemoglobin, were investigated by absorption and fluorescence spectrometry. To quantify the experimental results on hypericin release, here we use a kinetic curves fitting approach and calculate hypericin release rates in different environments. This approach allows to compare various mathematical models and uses more parameters to better characterize drug release profiles. In addition, magnetic CZ particles were fabricated and proposed as a promising material for drug delivery and controlled release in biological systems. Optical spectrometry and MPM are effective approaches that may reveal potential of natural zeolites in controlled drug delivery and biomedical imaging. [DOI: 10.1117/1.JBO.23.9.091411]

Keywords: multiphoton microscopy; zeolite; clinoptilolite; hypericin; tendon.

Paper 180027SSRR received Jan. 15, 2018; accepted for publication May 15, 2018; published online Jun. 1, 2018.

1 Introduction

Controlled transport and release of functional compounds with the optimal rate is a promising area in modern medical and pharmaceutical research. It is anticipated that targeted delivery of bioactive preparations and their operated activation reduce treatment period and adverse effects. Porous nano/microparticles are considered as very perspective transporters for drug delivery. Among different types of porous materials, zeolites (ZLs), hydrated microporous aluminosilicate minerals, occupy a special place. The essential crystalline structure of ZL is three-dimensional (3-D) tetrahedral framework of oxygen-sharing AlO_4 and SiO_4 groups. Substitution of Al for Si in naturally occurring ZLs leads to charge imbalance and presence of other metal ions, typically mono- or divalent ions such as Ka, Na, Ca, Mg, and Ba. As a consequence, natural ZLs get negative charge, and the pores formed by the framework units have diameters ranging from ~3 to 12 Å. There are more than 40 types of natural ZLs, and as widespread low-cost porous minerals, they have been exploited in agricultural,[1,2] industrial,[1,3] and environmental[4–6] technologies for long period of time. Clinoptilolite (CZ), a hydrated alkali zeolite, is one of the widely used minerals in the ZL family. CZ belongs to heulandite type of ZLs and has the following general chemical formula: $(Na_2, K_2, Ca)_3Al_6Si_{30}O_{72} \cdot 24H_2O$.[7] The ratio Si/Al in CZ varies from 4.0 to 5.3. The adsorption properties of CZ have been investigated previously.[8,9] It is determined that the value of specific surface area is in the range of 10 to 16 m^2/g for different mineral deposits, and the mineral pore size (PS) distribution can be characterized by two narrow ($PS_1 < 2$ nm, $2 < PS_2 < 5$ nm) and one broad ($PS_3 > 5$ nm) curves.[8] The presence of several types of porosity is an important feature of CZ. The primary porosity with $PS_1 < 2$ nm is caused by the specific crystal building of CZ grains, and the system of meso- and macropores (secondary porosity, with PS_2 and PS_3) is related to sizes and structural features of CZ mineral grains in the rock.[8]

CZ has chemically neutral basic structure and high resistance to extreme temperatures. As a biochemical sieve, feed and food additive, gas and odor absorber, CZ is widely used in agriculture, medicine, pollution control, and food industry. CZ is a very effective ion exchanger, it is used to remove radioactive ^{137}Cs and ^{90}Sr from nuclear waste and fallout,[10,11] and ammonia from sewage streams.[6] Pharmacological and clinical studies demonstrate that CZ is inert, does not produce biological damage to humans, and modified CZs have antimicrobial, gastric antacid, antidiarrheic, and antihyperglycemic features.[12] Clinically formulated CZ products are commercially available in the United States and Europe.

Although a handful of physical properties of zeolite have been studied using optical spectroscopy, x-ray, AFM, and SEM, the mechanisms of its biomedical effects are yet to be investigated and can be facilitated by optical imaging tools for biomedical and pharmacological application. CZ particles

*Address all correspondence to: Shean-Jen Chen, E-mail: sheanjen@nctu.edu.tw

1083-3668/2018/$25.00

are nearly transparent crystals of monoclinic symmetry. Some colors of CZ (e.g., brown, pink, and red) refer to impurities such as iron oxide. Luminescence properties of natural CZs were investigated earlier, and the UV-blue (220 to 420 nm) band with maximum at around 280-nm excitation spectrum and broad emission band (300 to 600 nm) were observed.[13–15] It was demonstrated that CZ luminescence depended on local defects and imperfections in crystals.[13] Substitution of Fe^{3+} ions with ions of other metals formed the centers of luminescence, and high correlation in the emission intensity around 350 nm with the Fe^{3+} concentration was observed in the specimen. This happened when iron ions substituted aluminum ions in the tetrahedral aluminum-silicate framework. Other factors and imperfections, such as interstitial atoms and ions, decationization and dihydroxylation, phonon, electron, and hole excitons can also be responsible for luminescence of CZ.[13] Furthermore, intensity increase in photoluminescence with the enrichment of CZ in raw mineral or during irradiation of the CZ samples by low dose of accelerated electrons (8 MeV) was observed.[15] The formation of luminescence centers was explained by radiation-induced change of the lattice ions and emergence of oxygen-cation vacancy. However, the scattering and linear absorption of zeolites samples are very strong in the UV spectral region and hinder to perform conventional spectroscopic measurements or optical imaging. Recently, the first effort of multiphoton imaging of CZ nano/microparticles has been performed, and a method of quantitative study of loading and release of photodynamic dyes by nano/microsized CZ particles using multiphoton microscopy (MPM) and optical spectrometry has been suggested.[16] Here we propose a new, more general method for quantification of the adsorbed dye release, and perform more detailed investigation of the release of a natural photodynamic pigment hypericin from CZ nano/microparticles.

2 Materials and Methods

2.1 *Preparation of the Clinoptilolite Zeolite*

Zeolite samples of CZ type, originating from Noyemberyan, Armenia, were used in the study. Mineral analysis using x-ray diffraction showed that zeolite samples consisted of ~90% CZ. Zeolite mineral was ground to 30 to 50 μm by a mortar, purified by washing with distilled water using a fluidized bed process, and then dried at 105°C. Deionized water was used in the processing. Nano/microsized CZ particles were obtained by grinding of minerals in a jet mill with subsequent sedimentation in aqueous solution. Particle size was then determined using a particle size analyzer (Malvern Zetasizer 3000, United Kingdom).

2.2 *Preparation of Magnetic Carriers Based on the CZ-Fe_3O_4 Composite*

Magnetic iron oxide Fe_3O_4 (IO) nanoparticles with diameter of 6.5 ± 3 nm was purchased from Sigma-Aldrich (Cat #07318), and oleic acid was used as surfactant for the stabilization. Magnetic composites were prepared by mixing the IO nanoparticles and aqueous solution of CZ and evenly dispersed with ultrasonic. The amount of IO was adjusted to obtain IO/CZ weight ratio of 1:10. By a simple magnetic procedure, the obtained composites were separated from nonmagnetic particles and dried in an oven at 90°C. The magnetism of samples was measured by a Lake Shore 7400 vibrating sample magnetometer at room temperature with the magnetic field of 20 kOe.

The saturation magnetization was about 3.7 $A \cdot m^2/kg$. The as-prepared composites were transferred into air-tight containers and kept in the dark.

2.3 *Photosensitizers and Biomolecules*

Photodynamic dyes [hypericin (HYP), methylene blue (MB), chlorin e_6, and fluorescein), biomolecules [collagen from bovine Achilles tendon (BAT), bovine hemoglobin, human serum albumin (HSA)] and chemical reagents from Sigma–Aldrich were of analytical grade (AR grade) and used without further purification. HYP powder was dissolved in dimethyl sulfoxide (DMSO) and stored at 4°C. In the experiments, HYP stock solution diluted to 5 μM in phosphate-buffered saline (PBS, pH 7.4). Other photodynamic dyes were water-soluble and dissolved in PBS.

Adsorption properties of CZ were studied using a batch equilibrium technique by placing CZ particles in a glass bottle containing 1, 2, 4, and 6 μM initial concentrations of the dye solution in PBS. The equilibrium concentrations of dyes were determined by absorption measurements at characteristic wavelengths using the DU 800 UV/VIS (Beckman Coulter, Inc.) spectrophotometer. The calibration curves for each dye at the respective wavelengths were established as a function of dye concentration. In the experiments, adsorbents were separated from solutions by gravity, and the concentration of the remaining dye solutions was obtained using calibration curves. The amount of adsorbed dye was determined by the difference between the initial and remaining concentrations of the dye solution. The adsorption capacity was calculated using parameters: concentration of adsorbed dye, solution volume, and adsorbent mass. Deionized water with $>6 \times 10^{-8}$ Siemens/cm conductivity value was used in the experiments.

2.4 *Spectrometry and Multiphoton Microscopy*

Optical properties of CZ and their composites with dyes were characterized by "SpectraSense" spectral acquisition and data processing system (Princeton Instruments, Acton) and DU 800 UV/VIS (Beckman Coulter, Inc.) spectrophotometer, spectral resolution was 1 nm.

Multiphoton imaging was performed by laser scanning microscope LSM 510 META (Carl Zeiss, Jena, Germany) coupled to the Ti:sapphire fs Tsunami laser, operating at 730- to 850-nm wavelength region, with pulsewidth of 120 fs and repetition rate of 80 MHz. The average power at the sample was between 5 and 10 mW. Detection bandwidths for second-harmonic generation (SHG) and two-photon excited luminescence (TPEL) signals were 380 to 400 nm and 420 to 650 nm, respectively, and detection parameters were detector gain: 850 V, ampl. offset: −0.5, ampl. gain: 1. Plan Neofluar air objectives $20\times/0.5$ NA, working distance WD = 1.3 mm and Fluar water immersion $40\times/1.2$ NA, WD = 0.28 mm (Carl Zeiss, Germany) objectives were used in the multiphoton imaging. The beam spot size near the focus of $40\times/1.2$ NA scanning objective lens was 340 nm and light intensity was $\sim 5.5 \cdot \times 10^{11}$ W/cm^2.

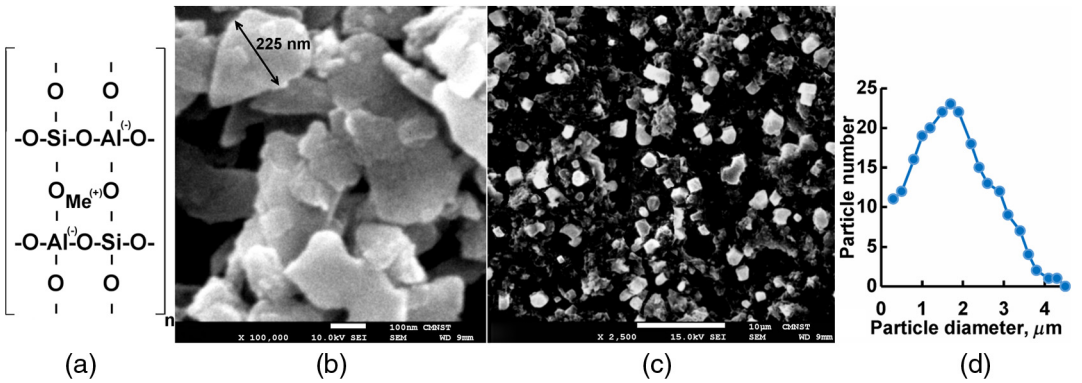

Fig. 1 (a) Basic structure of zeolite. SEM images of CZ (b) nano- and (c) microparticles. (d) CZ microparticle size distribution.

3 Results

3.1 *SEM and Multiphoton Microscopy of Clinoptilolite*

Basic structure of zeolite is shown in Fig. 1(a), and sizes and morphology of CZ nano/microparticles are examined by SEM [Figs. 1(b) and 1(c)]. Nanosized CZ particles have tablet-like form, with characteristic size about 225 nm [Fig. 1(b)]. In the case of high concentration, some aggregation of particles is observed, and these tablets merge along their bases. The shape of CZ microparticles can be characterized as prism with characteristic size <3 μm; however, part of particles has curved morphology [Fig. 1(c)]. SEM imaging of zeolite particles with low magnification is performed, and particle size distribution is measured using two to three images [Fig. 1(d)]. Mean sizes and standard deviations are 1.21 ± 0.15 μm and 230 ± 35 nm for micro- and nanoparticles, respectively.

Multiphoton imaging of unstained natural CZ revealed that bulk samples, as well as CZ nano/microparticles produced both SHG signal and TPEL at fs near-infrared laser excitation. TPEL was detected by the 420- to 650-nm registration channel when excitation wavelength was <745 nm. At this wavelength range of excitation, no signal was detected by the SHG (380 to 400 nm) registration channel. Nor any reliable signal was registered at excitation by 745- to 760-nm laser wavelength, and a strong, polarization-depended signal was registered by the SHG channel at excitation with 760- to 800-nm fs laser. The results obtained at 740- and 780-nm excitations are merged into Fig. 2, where SHG signal (red pseudocolor) is seen inside TPEL (green pseudocolor) regions. These multiphoton imaging can be interpreted as a formation of TPEL when excitation wavelength was shorter than 745 nm and the generation of second-harmonic signal in CZ particles when excitation wavelength was in the 760- to 800-nm range. In addition, multiphoton imaging allowed to measure sizes of CZ microparticles and estimate upper limit of the diameter of nanosized CZ particles.[16]

3.2 *Adsorption Properties of CZ Particles*

Magnetic nano/microparticles were prepared by incorporation of IO nanoparticles into the CZ matrix to enhance their physical properties and expand area of biomedical applications. The fabricated IO-CZ nano/microparticles preserve their magnetic and adsorption characteristics at least for 9 months. Magnetic IO-CZ particles can be easily separated from nonmagnetic CZ or other

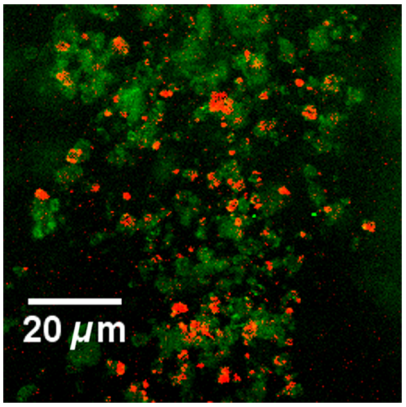

Fig. 2 TPEL (green pseudocolor, excitation wavelength: 740 nm) and SHG (red pseudocolor, excitation wavelength: 780 nm) imaging of CZ microsized particles.

nonmagnetic materials in few minutes (see Fig. 3). In addition, it is shown that the temperature of the aqueous suspension of CZ-IO composite of 2 cm^3 can be increased by 7°C in 3 min by an induction heater.

Multiphoton imaging allowed to investigate the interaction of individual CZ particles with biomolecules and dyes in different media and conditions. A series of experiments was performed to

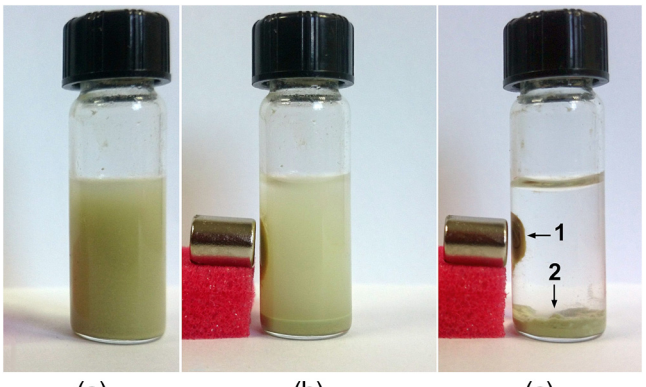

Fig. 3 Separation of (1) magnetic iron oxide-CZ particles from (2) nonmagnetic CZ particles: (a) before applying magnetic field, (b) after 0.5 and (c) 8 min application of the magnetic field.

characterize CZ adsorption properties of some effective photosensitizers: hypericin (HYP), methylene blue (MB), and fluorescein. These dyes have strong antimicrobial-anticancer properties. Therefore, CZ adsorption capacity to these dyes and possibility of their release in different environmental conditions are of interest to biomedicine.

Using the batch equilibrium technique method described in Sec. 2.3, it was shown that CZ particles effectively adsorbed MB (a cationic dye), HYP (a hydrophobic dye), and chlorin e_6 (a neutral dye) and did not adsorb fluorescein (an anionic dye) dissolved in PBS. These results were confirmed by MPM. In Fig. 4, the red pseudocolor is used to visualize CZ particles by the SHG imaging, and green pseudocolor is used to register localization of dyes by the TPEL imaging. In Fig. 4(a) only SHG signal can be seen from CZ microparticles on the surface of a microscope slide. After adding a droplet of MB to the slide, one can see that almost all the dye molecules are adsorbed by CZ particles, and individual particles emit strong two-photon excited fluorescence [Fig. 4(b)]. Simultaneously, the SHG signal from CZ particles is practically quenched. A completely different pattern was observed when a droplet of nonadsorbing fluorescein was added to the slide.[16] In this case, TPEL of fluorescein molecules has roughly uniform distribution, and CZ particles do not accumulate anionic fluorescein molecules in contrast to cationic MB, and SHG radiation from CZ particles is not quenched by fluorescein molecules.[16]

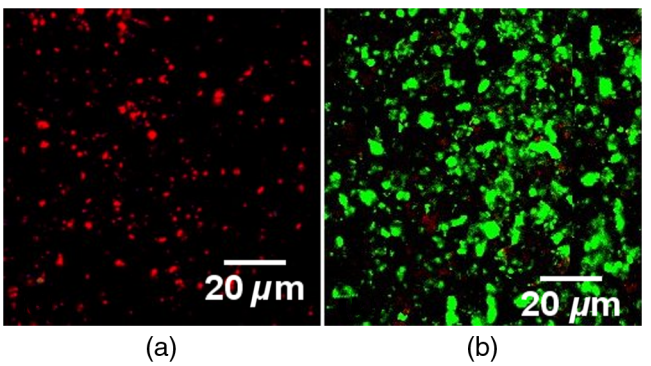

Fig. 4 Multiphoton imaging of the CZ-dye interaction. (a) Pure CZ microparticles produce only SGH signal at 780-nm fs excitation. (b) Only two-photon excited fluorescence is observed from CZ particles when they adsorb MB molecules.

Similar multiphoton imaging showed that CZ effectively adsorbed photodynamically active HYP from aqueous solutions. Taking into account the sizes of the used dyes, one can make preliminary conclusion that the mesoporosity, negative charge of CZ, and hydrophobicity of dyes play main role in adsorption processes in CZ-dye systems.

HYP was widely used in photodynamic therapy and fluorescence diagnostics of cancer, and we investigated the interaction of HYP + CZ particles with biomacromolecules such as BAT, HSA, and bovine hemoglobin in more detail. Adsorption of HYP by CZ particles was characterized as follows: CZ nanoparticle suspension with concentration of 1.2 g/l accumulated ~90% of HYP molecules from PBS solution with the concentration of $5 \cdot \times 10^{-6}$ M. HYP + CZ composite was stable in PBS, it had weak, nonstructured absorption spectrum [Fig. 5(a), curve 1], and weak broadband fluorescence near 600 nm. However, the addition of ethanol (EtOH) or DMSO to the HYP + CZ suspension resulted in gradual desorption of the HYP aggregates from CZ particles, and their disaggregation in EtOH or DMSO solutions. In case of addition of biomacromolecules to the HYP + CZ system, a release of HYP and binding to the organic molecules occurred. HYP disaggregation in the solvent and binding to biomacromolecules are accompanied by some changes in the absorption spectrum [Fig. 5(a)] and a significant increase in the fluorescence intensity of the dye [Fig. 5(b)].

Spectral properties of HYP allowed to study the rate of HYP adsorption, release, and binding to organic molecules. The kinetic of HYP release and binding in HYP + CZ + BAT system were investigated and quantified using kinetic spectrofluorometry. Fluorescence spectra of HYP + CZ system in PBS after addition of BAT (10^{-6} M) and release of HYP from zeolite pores measured by "SpectraSense" spectrofluorometer are presented in Fig. 6, where an increase in HYP fluorescence (in 570- to 670-nm spectral range), as well as a decrease and redshift of BAT fluorescence (in 350- to 500-nm spectral range) are observed [Fig. 6(a)]. Collagen fluorescence redshifting and quenching effects in the presence of HYP have been observed previously[17] and indicate the binding and incorporation of HYP

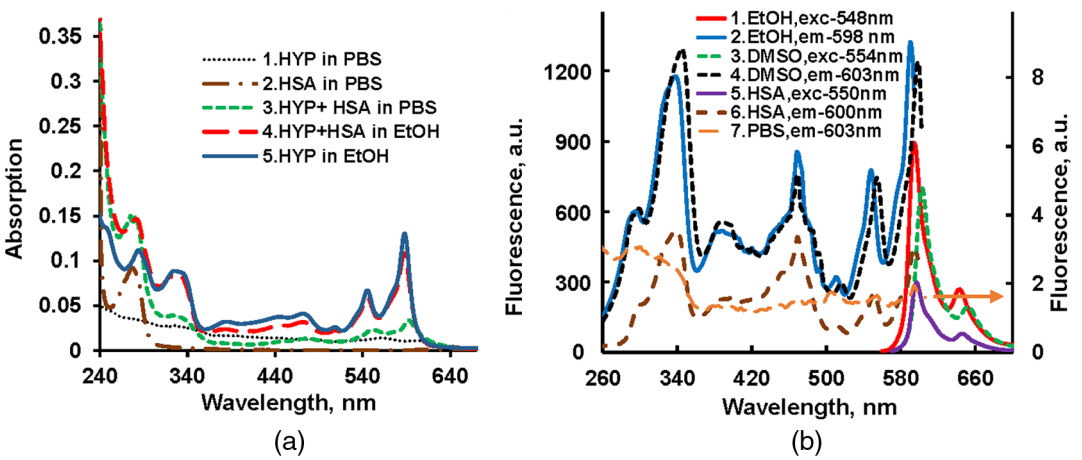

Fig. 5 (a) Absorption spectra of HYP as a function of the environment. The mole ratio between HYP and HAS for the line profiles 3 and 4 is 2:1. (b) Emission (1, 3, 5) and excitation (2, 4, 6, 7) spectra of HYP in (1, 2) EtOH, (3, 4) DMSO, (7) PBS, and (5, 6) after binding to HSA.

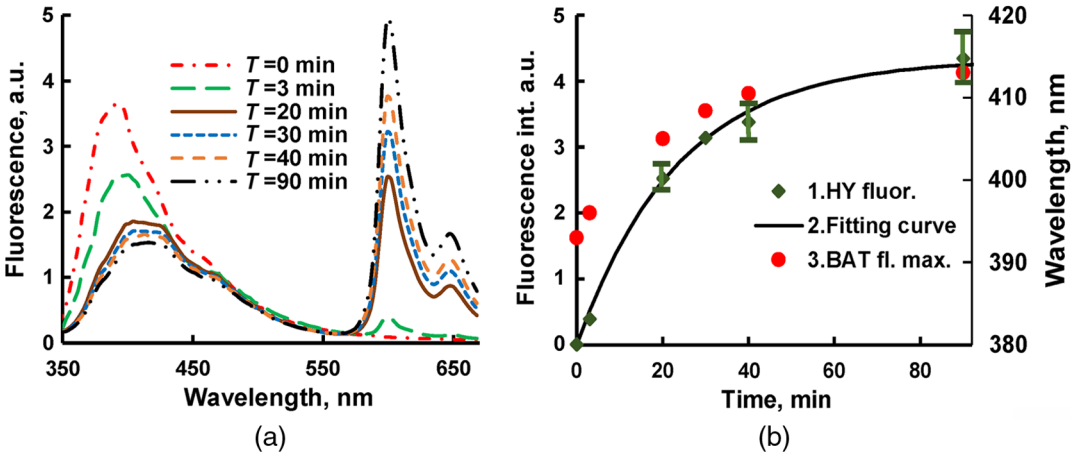

Fig. 6 (a) Time-dependent change of BAT (350 to 500 nm) and HYP (570 to 670 nm) fluorescence after addition of BAT to HYP-CZ system. Fluorescence excitation wavelength 330 nm. (b) (1) Kinetics of HYP release and fluorescence uprising after addition of BAT to HYP-CZ system. Fluorescence excitation and emission wavelengths are 550 and 600 nm, respectively. (2) Fitting curve for HYP fluorescence kinetics. (3) Time-dependent change of the maximum in BAT fluorescence spectrum.

molecules into collagen fiber. The experimental curve for HYP binding to BAT and fluorescence uprising is shown in Fig. 6(b), curve 1.

There are number of models to describe the drug release from controlled drug delivery systems.[18] For modellng and controlling the dye release, several parameters need to be determined.

If we assume that the HYP release from the CZ pores follows first-order kinetics, then the process can be expressed as[18]

$$\frac{dQ}{dt} = (Q_0 - Q)K, \tag{1}$$

where Q is the concentration of HYP molecules released in time t, Q_0 is the maximal concentration of released HYP, and K is the first-order release constant. From Eq. (1)

$$Q = Q_0[1 - \exp(-Kt)]. \tag{2}$$

For determination of the dye release rate, parameters K and Q_0 have been derived using built-in fitting function in Origin 8 Nonlinear Curve Fitting tool. The first-order release rate constant, K, after fitting the experimental data [Fig. 6(b)] with Eq. (2) is 0.0415 ± 0.0037 min^{-1} for BAT.

Similar experiments showed that HYP molecules release rate from CZ pores in the presence of HSA and bovine hemoglobin with 0.059 ± 0.00525 and 0.0501 ± 0.00473 min^{-1}, respectively.

4 Discussion

Natural CZ and its modified versions are prospective materials for pharmaceutics and biomedicine due to their nontoxicity, thermal stability, chemical tailorability, biocompatibility, and capability to adsorb different molecules and biological objects into their micro- and mesopores.[19–21] CZ is safe for human. It is used as an adsorbent of toxic metals, radioactive elements, and free radicals. CZ is successfully applied also in drug delivery and wound treatment. Particularly, CZ was used as hosts for aspirin, doxorubicin, and paraquat molecules,[22–24] as transporter for controlled ibuprofen and anthelminthics delivery and release.[25] A distinctive feature for drug delivery is the CZ mesoporosity[9] that allows to adsorb and transport simultaneously several types of molecules, nanoparticles, and large biomolecules for different biomedical applications. In addition, simple modification of CZ allows a controlled change of micropore sizes and specific surface area without deformation of the CZ skeleton.[8] Moreover, CZ is an effective adjuvant in anticancer treatment.[26,27]

MPM allows to detect CZ samples in 3-D using near-infrared radiation and to image the interaction of individual nano/microparticles with dyes, to quantitatively investigate and understand the interaction of host CZ particles with specific guest compounds. The experimental results obtained in our study for the several dyes indicate that the adsorption of CZ essentially depend on polarity of the molecules. Negatively charged CZ particles enable effectively adsorb cationic molecules, poorly adsorb neutral molecules, and does not adsorb anionic molecules. The molecule loading-release characteristics depend on the CZ cation content and can be controlled by cation exchange.

More detailed research has been carried out on interaction of CZ with HYP, a natural pigment found in plants of the Hypericum genus. HYP has recently received increasing attention due to its high phototoxicity against viruses and malignant cells.[28–30] In addition, it has been shown that HYP is an effective sensitizer for selective light-controlled collagen modification in connective tissues,[31,32] which is important for therapy of collagen-related disorders and tissue engineering. However, HYP molecules aggregate in water or blood, form nonsoluble, nonfluorescent complexes, and lose photosensitizing, antitumor properties.[33] To overcome this drawback, the polyvinylpyrrolidone (average Mw 40,000) has been tested as a water-soluble carrier enabling intravenous transportation of HYP.[34] Microporous CZ particles, as more universal transporter for systemic application of HYP, was suggested and quantitatively investigated previously.[16] Absorption and fluorescence spectra of HYP strongly depend on molecular environments. Using this HYP feature, the rate of release of HYP from CZ particles in the presence of biomolecules was measured. Particularly, HYP release rates in the presence of BSA, collagen, human hemoglobin, and lipids were estimated applying the first-order kinetics model, where the logarithm of the dye concentration linearly depended on time. In this case, a simple graphical

method allowed to determine the release rate from the slope of the straight line and to calculate the R^2 correlation coefficient.[16] However, the first-order kinetics model and graphical method of quantification have limited application. In a recent study,[35] a drug release system based on bexarotene-loaded CZ was quantitatively investigated by an HPLC-DAD method, and it was shown that depending on the type of drug immobilization, the release process was well described either by a first-order kinetic model or by the Korsmeyer–Peppas model. In the first model, the drug release rate is constant, whereas in the second model the release rate is a function of time. Furthermore, the first-order kinetics model cannot be used, when the temperature of the system changes, or there are several types of pores with different release rates. To quantify the experimental results, a kinetic curves fitting method is used here, which allows to apply more parameters to characterize release profiles. In addition, this more general approach permits to compare various mathematical models and select the most reliable model that provides the best specification of a drug release system. Moreover, this approach requires relatively short time for fluorescence measurements compared to the approach described in the previous publication,[16] which is important factor in *in vivo* experiments.

In these experiments, we use collagen from BAT that mainly consists of collagen type I. The type I collagen is the main collagen component of cornea, skin, bone, cartilage, and other fibrous connective tissues. The used collagen preparation is insoluble in water, aqueous buffers, and organic solvents, and the smaller release rate of HYP in the presence of type I collagen may be due precisely to this feature of the macromolecule.

In addition to adsorption/release experiments, we fabricated magnetic CZ particles to develop a new multifunctional magnetic and optical probe. The magnetic CZ composites exhibit strong and stable magnetic properties, which allow to separate these particles from other materials, and may be used in controlled drug delivery and MRI in the future.

Recently, different nanozeolites with magnetic nanocomposites were synthesized and their suitability for doxorubicin loading was studied.[36] None of the zeolites or magnetic nanocomposites showed toxicity to experimental cancer cells, and zeolite-based magnetic composites were considered as biocompatible medical devices, which can be used for efficient loading and slow release applications. In addition, it was revealed that artificial zeolites synthesized with magnetic NPs had strong magnetic properties, which allowed to manipulate them, separate from other materials, and use in MRI.[37] Furthermore, the performance of hydroxyapatite-based magnetic nanoparticles in *in vivo* cancer hyperthermia was demonstrated.[38] In order to achieve hyperthermia, the mice were placed into a 3-cm-diameter coil of an inductive heater. Only the mice which were injected with magnetic nanoparticles and had been treated by alternating magnetic field showed dramatic reduction of tumor volume. No recurrence of tumor was noted. In these experiments, the temperature was raised from 38°C to 44°C within 5 min and kept in the desired temperature interval (45 to 46°C) for 15 min.[38]

5 Conclusion

Nonlinear optical properties of CZ type of natural zeolite allowed to use the MPM in imaging of CZ nano/microparticles, and visualizing of dye adsorption/desorption processes. The dynamic interaction of CZ-dye complexes with biomolecules was quantified using fluorescence and absorption spectrometry. A method of magnetic CZ particles fabrication was developed and some magnetic properties were demonstrated. Magnetic CZ nano/microparticles can be considered as new multimodal probes for optical imaging and MRI, thermo- and phototherapy and as effective containers for controlled drug delivery. Further *in vivo* studies are needed to evaluate the efficacy of magnetic CZ nano/microparticles in cancer hyperthermia therapy.

Disclosures

The authors have no relevant financial interests in this article and no potential conflicts of interest to disclose.

Acknowledgments

This study was financially supported by the Ministry of Science and Technology, Taiwan (MOST 107-2923-E-009-00333 and MOST 106-2320-B-006-061).

References

1. F. A. Mumpton, "La roca magica: uses of natural zeolites in agriculture and industry," *Proc. Natl. Acad. Sci. U. S. A.* **96**, 3463–3470 (1999).
2. M. Rehakova et al., "Agricultural and agrochemical uses of natural zeolite of the clinoptilolite type," *Curr. Opin. Solid State Mater. Sci.* **8**, 397–404 (2004).
3. J. E. Naberde et al., "Industrial applications of zeolite catalysis," *Stud. Surf. Sci. Catal.* **84**, 2197–2219 (1994).
4. C. Colella, "Applications of natural zeolites," in *Handbook of Porous Solids*, F. Schüth, K. S. W. Sing, and J. Weitkamp, Eds., pp. 1156–1189, Wiley-VCH, Weiheim, Germany (2002).
5. R. S. Bowman, "Application of surfactant-modified zeolites to environmental remediation," *Microporous Mesoporous Mater.* **61**, 43–56 (2003).
6. W. H. Tian and X. H. Wen, "Using a zeolite medium biofilter to remove organic pollutant and ammonia simultaneously," *J. Environ. Sci.-China* **16**, 90–93 (2004).
7. C. Baerlocher, L. B. McCusker, and D. H. Olson, *Atlas of Zeolite Framework Types*, 6th revised ed., pp. 156–157, Elsevier, Amsterdam, The Netherland (2007).
8. O. Korkuna et al., "Structural and physicochemical properties of natural zeolites: clinoptilolite and mordenite," *Microporous Mesoporous Mater.* **87**, 243–254 (2006).
9. K. Möller and T. Bein, "Mesoporosity: a new dimension for zeolites," *Chem. Soc. Rev.* **42**, 3689–3707 (2013).
10. E. Johan et al., "Natural zeolites as potential materials for decontamination of radioactive cesium," *Proc. Environ. Sci.* **28**, 52–56 (2015).
11. H. Yeritsyan et al., "Radiation-modified natural zeolites for cleaning liquid nuclear waste (irradiation against radioactivity)," *Sci. Rep.* **3**, 2900 (2013).
12. B. Kwakye-Awuah et al., "Antimicrobial action and efficiency of silver-loaded zeolite X," *J. Appl. Microbiol.* **104**, 1516–1524 (2008).
13. M. S. Joshi and B. T. Bhoskar, "Luminescence studies on zeolite crystals," *Crystal Res. Technol.* **18**, 213–218 (1983).
14. H. Maas, A. Currao, and G. Calzaferri, "Encapsulated lanthanides as luminescent materials," *Angew. Chem. Int. Ed.* **41**, 2495–2497 (2002).
15. H. Yeritsyan et al., "The effect of electron irradiation on the optical properties of the natural Armenian zeolite-clinoptilolite," *Cent. Eur. J. Phys.* **3**, 623–635 (2005).
16. V. Hovhannisyan, C. Y. Dong, and S. J. Chen, "Photodynamic dye adsorption and release performance of natural zeolite," *Sci. Rep.* **7**, 45503 (2017).
17. D. Yova, V. Hovhannisyan, and T. Theodossiou, "Photochemical effects and hypericin photosensitized processes in collagen," *J. Biomed. Opt.* **6**(1), 52–57 (2001).
18. S. Dash et al., "Kinetic modeling on drug release from controlled drug delivery systems," *Acta Pol. Pharm.* **67**, 217–223 (2010).
19. T. Faras, A. R. Ruiz-Salvador, and A. Rivera, "Interaction studies between drugs and a purified natural clinoptilolite," *Microporous Mesoporous Mater.* **61**, 117–125 (2003).

20. M. Rahimi et al., "Zeolite nanoparticles for selective sorption of plasma proteins," *Sci. Rep.* **5**, 17259 (2015).
21. Z. Adamis et al., "In vitro and in vivo tests for determination of the pathogenicity of quartz, diatomaceous earth, mordenite and clinoptilolite," *Ann. Occup. Hyg.* **44**, 67–74 (2000).
22. H. Zhang, Y. Kim, and P. K. Dutta, "Controlled release of paraquat from surface-modified zeolite Y," *Microporous Mesoporous Mater.* **88**, 312–318 (2006).
23. M. Arruebo et al., "Sustained release of doxorubicin from zeolite-magnetite nanocomposites prepared by mechanical activation," *Nanotechnology* **17**, 4057–4064 (2006).
24. Q. Zhu et al., "Extracellular control of intracellular drug release for enhanced safety of anti-cancer chemotherapy," *Sci. Rep.* **6**, 28596 (2016).
25. D. Krajišnik et al., "Ibuprofen sorption and release by modified natural zeolites as prospective drug carriers," *Clay Miner.* **50**, 11–22 (2015).
26. K. Pavelić et al., "Natural zeolite clinoptilolite: new adjuvant in anticancer therapy," *J. Mol. Med.* **78**, 708–720 (2001).
27. N. Zarkovic, "Anticancer and antioxidative effects of micronized zeolite clinoptilolite," *Anticancer Res.* **23**, 1589–1595 (2003).
28. P. F. C. Menezes et al., "Photodynamic activity of different dyes," *Laser Phys.* **17**, 468–471 (2007).
29. P. Miskovsky, "Hypericin: a new antiviral and antitumor photosensitizer: mechanism of action and interaction with biological macromolecules," *Curr. Drug Targets* **3**, 55–84 (2002).
30. M. Van de Putte et al., "Elucidation of the tumoritropic principle of hypericin," *Br. J. Cancer* **92**, 1406–1413 (2005).
31. V. Hovhannisyan et al., "Hypericin-mediated selective photomodification of connective tissues," *Appl. Phys. Lett.* **105**, 263701 (2014).
32. V. Hovhannisyan et al., "Photo-induced processes in collagen-hypericin system revealed by fluorescence spectroscopy and multiphoton microscopy," *Biomed. Opt. Express* **5**, 1355–1362 (2014).
33. M. Van De Putte et al., "The impact of aggregation on the biodistribution of hypericin," *Int. J. Oncol.* **28**, 655–660 (2006).
34. A. Kubin et al., "How to make hypericin water-soluble," *Pharmazie* **63**, 263–269 (2008).
35. L. Ochiuz et al., "Development of a modified-release drug delivery system with bexarotene loaded in clinoptilolite," *Mater. Plast.* **54**, 581–585 (2017).
36. B. Divband et al., "Linde type A and nano magnetite/NaA zeolites: cytotoxicity and doxorubicin loading efficiency," *Open Chem.* **16**, 21–28 (2018).
37. E. Csajbok et al., "Gadolinium(III)-loaded nanoparticulate zeolites as potential high-field MRI contrast agents: relationship between structure and relaxivity," *Chem.-Eur. J.* **11**, 4799–4807 (2005).
38. C. H. Hou et al., "The in vivo performance of biomagnetic hydroxyapatite nanoparticles in cancer hyperthermia therapy," *Biomaterials* **30**, 3956–3960 (2009).

Biographies for the authors are not available.